JM PAPERS

Extreme wave statistics of surface elevation and velocity field of gravity waves over a two-dimensional bathymetry

Christopher Lawrence[1], Karsten Trulsen[1],† and Odin Gramstad[2]

[1]Department of Mathematics, University of Oslo, 0316 Oslo, Norway

[2]Hydrodynamics, Metocean and SRA, Energy Systems, DNV, 1322 Høvik, Norway

This paper presents the effects of two-dimensional bathymetry on the evolution of skewness and kurtosis of the surface elevation and velocity field in long-crested irregular waves propagating over a circular shoal and a submerged bar with a semicircular step. For a circular shoal, we show that the surface elevation has a local maximum of skewness and kurtosis on top of the shoal. We find that the skewness of the horizontal velocity field has similar behaviour to the surface elevation, but the kurtosis of the horizontal velocity field has two local maxima at different locations on the lee side of the shoal. For a semicircular step, which acts similar to a converging lens, we find that refraction contributes to the statistical properties of the surface elevation and horizontal velocity field to deviate from Gaussian statistics.

1. Introduction

Rogue waves are unusually large waves whose wave heights or crest heights are much larger than their surroundings. Haver (2000) suggested as criteria for a rogue wave event within a 20 minute time series of ocean surface waves that the crest height is larger than five quarters of the significant wave height, $\eta_{max} > 1.25H_s$, or the wave height is larger than twice the significant wave height, $H > 2H_s$. One physical mechanism that can produce rogue waves is spatial focusing, see Dysthe, Krogstad & Müller (2008). As waves propagate into shallower water, the presence of bottom topography affects the waves through shoaling and refraction. Refraction of waves can lead to spatial focusing of wave

† Email address for correspondence: karstent@math.uio.no

energy and, thus, enhance nonlinearity that may provoke non-Gaussian statistics. Rogue waves can occur not only in surface elevation, but also in other quantities such as the velocity field.

The deviation from Gaussian statistics provoked by a sloping bottom was found in field observations before it was measured in the laboratory. In her pioneering work, Bitner (1980) reported a field experiment of waves propagating into shallower water. Similar field experiments were later reported by Cherneva *et al.* (2005) and Teutsch *et al.* (2020). From a field data set in the southern North Sea, Teutsch *et al.* (2020) found that there was one buoy that captured more rogue waves than expected and it was located at a rather shallow water depth. Noticeable deviation from Gaussian statistics was found.

Laboratory work not considering statistics include the experiments of waves propagating over a submerged bar of Grue (1992) and Beji & Battjes (1993) who showed the growth of bound harmonics triggered by bottom topography. The experiment of Whalin (1971) considered harmonic wave propagating over a sloping bottom with parallel semicircular contours symmetric in the centre to study the nonlinear effects from the bottom combined with wave refraction. The experiment of Berkhoff, Booij & Radder (1982) had an elliptical shoal on the sloping bottom and the waves propagated with an angle. All of the wave tank experiments mentioned previously are widely used as benchmark tests for the validation of deterministic wave models.

Large values for skewness and kurtosis in finite and shallow water depth were observed initially in the laboratory experiment of long-crested irregular waves propagating over a sloping bottom reported by Trulsen, Zeng & Gramstad (2012). As the waves propagate over a slope, there is a local maximum in the skewness and kurtosis of the surface elevation near the edge of the shallower side of the slope. This behaviour was also demonstrated in numerical simulations by Sergeeva, Pelinovsky & Talipova (2011), Gramstad *et al.* (2013), Viotti & Dias (2014), Majda, Moore & Qi (2019), Zhang *et al.* (2019), Zheng *et al.* (2020), Li *et al.* (2021*c*) and Lawrence, Trulsen & Gramstad (2021*b*) and in experiments as reported by Kashima, Hirayama & Mori (2014), Ma, Dong & Ma (2014), Bolles, Speer & Moore (2019), Zhang *et al.* (2019), Wang *et al.* (2020), Moore *et al.* (2020) and Li *et al.* (2021*a*). Curiously, in a deeper regime with milder slope, Zeng & Trulsen (2012) did not find this behaviour. Subsequently, Lawrence *et al.* (2021*b*) confirmed the results by Zeng & Trulsen (2012) with a more accurate simulation model.

In the work of Janssen, Herbers & Battjes (2008) and Janssen & Herbers (2009), they included refraction effect from the bottom topography to study the wave statistics with a frequency-angular spectrum model by Janssen, Herbers & Battjes (2006). For directional waves, but without refraction, Ducrozet & Gouin (2017) suggested the extreme wave activity is reduced.

A theoretical explanation was developed by Majda *et al.* (2019) based on statistical mechanics of the Korteweg–de Vries (KdV) system. They recognized that the most likely states minimise the Hamiltonian, which in deeper water is associated with minimising the variance of the surface slope, but in shallower water is associated with an increase in the surface displacement skewness, giving rise to the non-Gaussian statistics observed in a number of studies. Another explanation developed by Li *et al.* (2021*b*) suggested the anomalies arise from interaction between linear free and second-order bound waves and new second-order free waves generated due to the abrupt depth transition.

In addition to the surface elevation, other quantities such as fluid kinematics and wave forces are of interest. The deviation from Gaussian statistics of fluid velocity can be more pronounced in shallower water as pointed out in Song & Wu (2000). Numerical studies by Sergeeva & Slunyaev (2013) suggested that rogue waves usually have large magnitudes
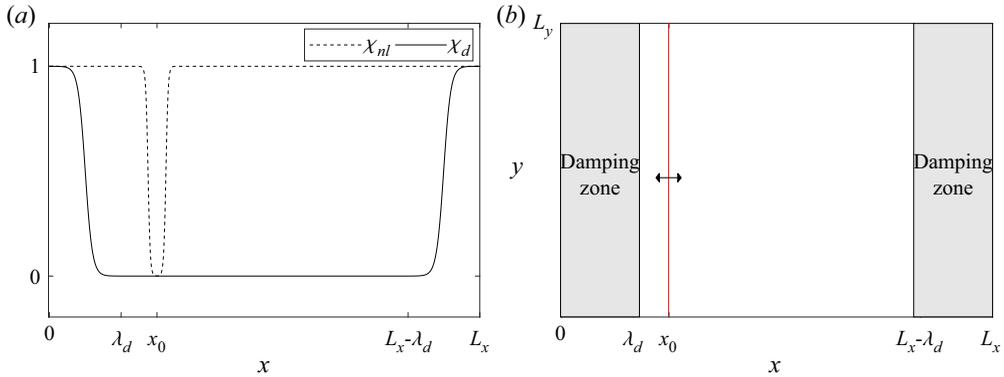
Figure 1. (*a*) Smooth functions χ_d for damping zones (solid line) and χ_{nl} for spatial nonlinear adjustment (dashed line). (*b*) Computational domain with damping zones and influx line (red) for wave generation.

of velocities, but large velocities do not necessarily correspond to rogue waves. Alberello *et al.* (2016) showed that the horizontal velocity is negatively skewed due to second-order effects. Through wave tank experiments of long-crested irregular waves over a shoal, Trulsen *et al.* (2020) found the kurtosis of the horizontal velocity can be different from the kurtosis of the surface elevation. For sufficiently shallow shoal, the kurtosis of the surface elevation has a local maximum near the edge of the slope on the incoming side, meanwhile the kurtosis of horizontal velocity has a local maximum on the downward slope on the lee side of the shoal. In the numerical simulations reported by Zhang & Benoit (2021) and Lawrence *et al.* (2021*b*), it was observed that strongly non-Gaussian statistics for both surface elevation and horizontal velocity fields are triggered by abrupt depth changes. Recent studies by Klahn, Madsen & Fuhrman (2021*a,b*) consider statistical properties of surface elevation, velocity field, acceleration and forces on a vertical column in deep water that show the deviation from Gaussian statistics as the wave steepness increases.

In this paper, we focus on two-dimensional bathymetry effects for the statistical properties of surface elevation and horizontal velocity field in long-crested irregular waves propagating over a circular shoal and submerged bar with a semicircular step. The organisation of the rest of the paper is as follows. In § 2, the numerical model for 3D nonlinear wave propagation for non-uniform bathymetry including the wave kinematics calculation is described. In § 3, the statistical moments and their convergence are presented. In § 4, we present the results of numerical simulation for evolution of the statistical moments through different bathymetries. Finally, a discussion and summary with conclusions are found in §§ 5 and 6, respectively.

2. Numerical model

2.1. *High-order spectral method*

We consider a 3D rectangular fluid domain, periodic in the horizontal directions and equipped with a Cartesian coordinate system, as shown in figure 1. Here $z = \eta(x, y, t)$ denotes the free surface elevation and $z = 0$ is the still water level. We use $z = -h_0 + \beta(x, y)$ to denote the bottom topography, where h_0 is the mean water depth and $\beta(x, y)$ is the bottom variation.

A potential theory is used assuming inviscid fluid and irrotational flow. The fluid velocity is expressed by the velocity potential ϕ, $V = \nabla \phi$. Assuming the fluid is

incompressible, the continuity equation becomes the Laplace equation

$$\nabla \cdot \nabla \phi = 0. \tag{2.1}$$

We consider periodic boundary conditions in the horizontal plane. The bottom boundary condition is

$$\nabla \phi \cdot \nabla \beta - \frac{\partial \phi}{\partial z} = 0 \quad \text{at } z = -h_0 + \beta(x, y). \tag{2.2}$$

As pointed out in Zakharov (1968), the kinematic and dynamic nonlinear free surface boundary conditions can be written in terms of surface elevation η and surface potential $\phi_s = \phi(x, y, z = \eta, t)$

$$\left.\begin{aligned}
\frac{\partial \eta}{\partial t} &= W \left(1 + |\nabla \eta|^2\right) - \nabla \phi_s \cdot \nabla \eta \\
\frac{\partial \phi_s}{\partial t} &= -g\eta - \frac{1}{2} |\nabla \phi_s|^2 + \frac{1}{2} W^2 \left(1 + |\nabla \eta|^2\right),
\end{aligned}\right\} \tag{2.3}$$

where g is the acceleration of gravity and $W = \partial \phi / \partial z|_{z=\eta}$ is the vertical velocity at the surface. The surface vertical velocity W needs to be evaluated to solve the system. For flat bottom, an efficient pseudo-spectral method to calculate the surface vertical velocity W in terms of η and ϕ_s was initially introduced by Dommermuth & Yue (1987) and West *et al.* (1987), and it has been known as the high-order spectral method (HOSM). Extension to variable depth was discussed in Gouin, Ducrozet & Ferrant (2016, 2017). A brief summary of the HOSM for variable depth by Gouin *et al.* (2017) is presented in the following.

The velocity potential ϕ is expressed as a truncated power series $\phi = \sum_{m=1}^{M} \phi^{(m)}$ where m is the nonlinear order of $\phi^{(m)}$ and M is the nonlinear order of the method which can be freely chosen. The velocity potential evaluated at the free surface ϕ_s is then expanded in a Taylor series around the still water level $z = 0$.

For an uneven bottom, an additional velocity potential ϕ_B is expressed as a truncated power series $\phi_B = \sum_{m=1}^{M} \phi_B^{(m)}$ and $\phi_B^{(m)} = \sum_{l=1}^{M_B} \phi_B^{(m,l)}$ where M_B is the order for the bottom boundary condition which can be different from M and can be freely chosen. Thus, the velocity potential $\phi^{(m)}$ is expressed as the sum of two components

$$\left.\begin{aligned}
\phi^{(m)} &= \phi_0^{(m)} + \phi_B^{(m)} \\
\phi_0^{(m)}(x, y, z, t) &= \sum_{p,q} A_{pq}^{(m)}(t) \frac{\cosh(k_{pq}(z + h_0))}{\cosh(k_{pq}h_0)} \exp(\mathrm{i}(k_{x_p}x + k_{y_q}y)) \\
\phi_B^{(m)}(x, y, z, t) &= \sum_{p,q} B_{pq}^{(m)}(t) \frac{\sinh(k_{pq}z)}{\cosh(k_{pq}h_0)} \exp(\mathrm{i}(k_{x_p}x + k_{y_q}y))
\end{aligned}\right\} \tag{2.4}$$

with $k_{x_p} = (p - N_x/2 + 1)(2\pi/L_x)$ for $p = 0, \ldots, N_x - 1$, $k_{y_q} = (q - N_y/2 + 1)(2\pi/L_y)$ for $q = 0, \ldots, N_y - 1$ and $k_{pq} = \sqrt{k_{x_p}^2 + k_{y_q}^2}$. Here N_x and N_y are the number of wave components in the x and y directions, respectively. We choose N_x and N_y to be even numbers. We use $A_{pq}^{(m)}(t)$ and $B_{pq}^{(m)}(t) = \sum_{l=1}^{M_B} B_{pq}^{(m,l)}(t)$ to denote the modal amplitudes of $\phi_0^{(m)}$ and $\phi_B^{(m)}$, respectively. With the velocity potential in (2.4) and Taylor expansion of the bottom boundary condition in (2.2), we can calculate each $B_{pq}^{(m,l)}(t)$.

For evaluation of the vertical velocity at the surface, W, a similar expansion series of surface potential is applied for the vertical velocity at the surface $W = \sum_{m=1}^{M} W^{(m)}$.

Then, Taylor expansion around the still water level $z = 0$ leads to a triangular system for $W^{(m)}$ to be solved iteratively. Once the vertical velocity at the surface $W^{(m)}$ has been computed, then the free surface elevation η and surface potential ϕ_s can be marched in time through (2.3).

This method is based on a Taylor expansion of the bottom boundary condition with respect to the mean water depth and solved numerically by pseudo-spectral method. The bottom and its gradient need to be continuous to avoid any instabilities. For larger bottom variation β/h_0, the error on the vertical velocity at the surface, W, becomes larger and the convergence is slower but still exists by increasing number of wave components and orders of the method M and M_B. A detailed convergence study in one horizontal dimension with respect to the number of wave component N_x and orders M and M_B is presented for variable depth in Gouin *et al.* (2016).

2.2. *Wave generation and damping zones*

For a flat bottom, the simulation can be initiated by specifying the surface elevation η and the surface potential ϕ_s at initial time $t = 0$. The prescribed initial condition has to be periodic because of the pseudo-spectral method. For an uneven bottom, it is convenient to start simulations from rest ($\eta = \phi_s = 0$) and use a wave generator inside the domain. Embedded wave generation is implemented with spatial nonlinear adjustment as described in Lie, Adytia & van Groesen (2014). To ensure the periodicity, a couple of damping zones of length λ_d are also applied.

The dynamic equations with embedded wave generation and damping zones become

$$\left.\begin{aligned} \frac{\partial \eta}{\partial t} &= RHS_{lin} + RHS_{nonlin}\chi_{nl} - c_d\eta\chi_d + S_{x_0} \\ \frac{\partial \phi_s}{\partial t} &= RHS_{lin} + RHS_{nonlin}\chi_{nl} - c_d\phi_s\chi_d \end{aligned}\right\} \tag{2.5}$$

where RHS_{lin} and RHS_{nonlin} are the linear and nonlinear parts of right-hand sides of the dynamic equations, c_d is the damping coefficient, S is the source term for embedded wave generation and χ_{nl} and χ_d are smooth functions. Illustration of the chosen functions for nonlinear adjustment and damping zones is shown in figure 1. In the damping zone, the solutions decay exponentially as $e^{-c_d T_d}$, where T_d is the travel time of the wave in the damping zone. The value of the damping coefficient c_d and the length of the damping zone λ_d are coupled. As an example, for exponential decay of $10^{-3} \approx e^{-7}$, the length of the damping zone should be at least $\lambda_d = 7V_g/c_d$, where V_g is the group velocity.

2.3. *Wave kinematics calculation*

The HOSM calculates the surface vertical velocity W in terms of surface elevation η and surface potential ϕ_s. For wave kinematics calculation, it is convenient to use (2.4) directly after the modal amplitudes A_{pq} and B_{pq} are known. We refer this method as the direct method in this paper. We consider a solitary wave and Stokes waves on a flat bottom to check the validity of the direct method.

Solitary waves with amplitude over depth $A/h = 0.4$ and $A/h = 0.6$ are chosen. We took the surface elevation and the surface potential for the solitary waves from the exact solution of the Euler equations by Dutykh & Clamond (2014) as input to calculate the interior horizontal velocity with the direct method. Figure 2 shows the comparison of the horizontal velocity profile of solitary wave at the crest by the direct method and the reference solution from Dutykh & Clamond (2014). For a rather extreme solitary wave
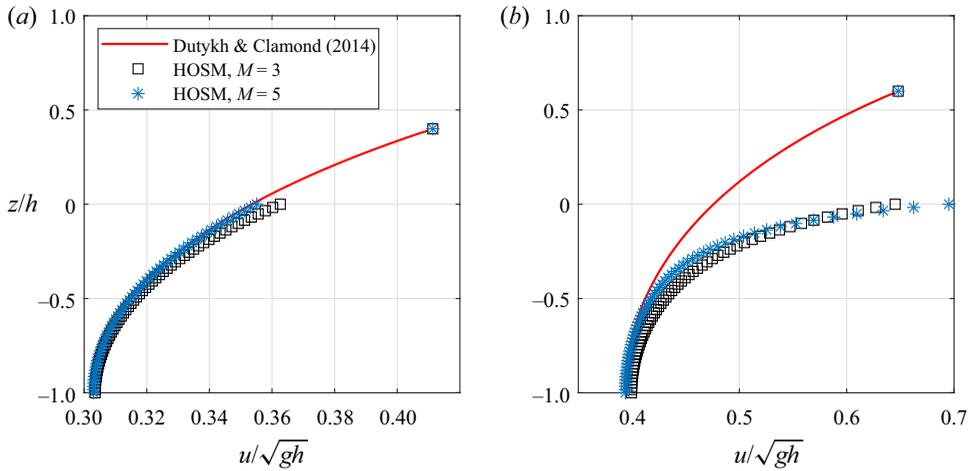
Figure 2. Horizontal velocity profiles of solitary waves with (*a*) $A/h = 0.4$ and (*b*) $A/h = 0.6$.
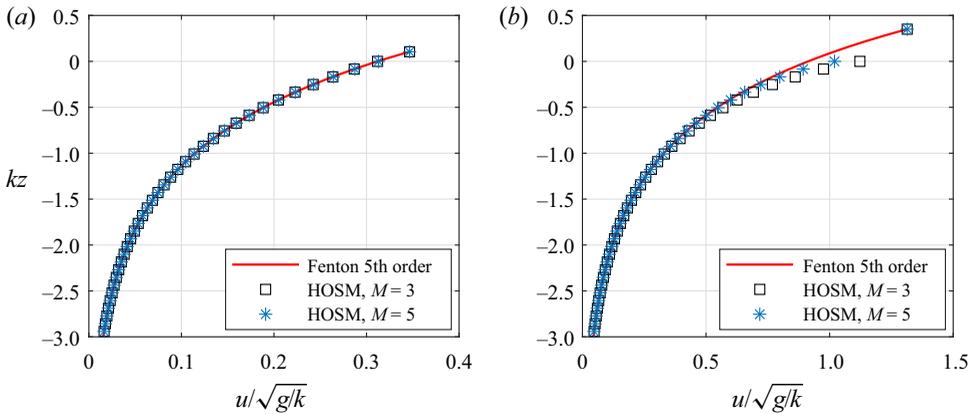

Figure 3. Horizontal velocity profiles of Stokes waves with (*a*) $ka = 0.1$ and (*b*) $ka = 0.3$.

$A/h = 0.6$, the direct method gives inaccurate horizontal velocity close to the surface. For a milder case $A/h = 0.4$, the accuracy of the direct method can be improved by increasing the nonlinear order.

We consider a Stokes waves in deep water ($kh = 10$) with $ka = 0.1$ and $ka = 0.3$, where a is the first-order amplitude, k is the wavenumber and h is the water depth. We use the fifth-order solution by Fenton (1985) to obtain the surface elevation and surface potential. The surface potential is calculated from the fifth-order velocity potential at $z = \eta$, retaining fifth-order terms. Figure 3 shows the comparison of horizontal velocity under the wave crest by the direct method with Fenton's solution. For Stokes wave with steepness $ka = 0.1$, the direct method gives a good agreement compared with Fenton's solution. Meanwhile, the horizontal velocity by the direct method starts to deviate from Fenton's solution close to the surface when the steepness is increased to $ka = 0.3$.

From both test cases, we see that the direct method is inaccurate to calculate the horizontal velocity near the surface for strongly nonlinear cases. However, the direct method is still valid down to the bottom and for low steepness parameter A/h in shallow

939 A41-6

water or *ka* in deep water. This problem has been pointed out in Bateman, Swan & Taylor (2003) where the H and H_2 operators were introduced. For flat bottom, the direct method is equivalent to the H operator method. The H_2 operator method was proposed in Bateman *et al.* (2003) as a remedy. For varying bottom, the more advanced variational Boussinesq model was proposed to calculate the wave kinematics in Lawrence, Gramstad & Trulsen (2021*a*).

In the present paper, we focus on the interior horizontal fluid velocity where it is not close to the water surface or the bottom. Therefore, we still use the direct method because it is efficient and sufficiently accurate to study the evolution of the statistical properties of velocity field.

3. Statistical moments

We focus on the third- and fourth-order moments of the surface elevation and horizontal velocity, the skewness and the kurtosis, respectively. The skewness and the kurtosis of the surface elevation are defined as

$$\text{skewness} = \frac{\mathrm{E}\left[(\eta - \mathrm{E}[\eta])^3\right]}{\sigma(\eta)^3}, \quad \text{kurtosis} = \frac{\mathrm{E}\left[(\eta - \mathrm{E}[\eta])^4\right]}{\sigma(\eta)^4}, \tag{3.1a,b}$$

where $\mathrm{E}[\cdot]$ denotes the expected value and $\sigma(\cdot)$ is the standard deviation. We have similar expressions for the horizontal velocity.

The skewness is a measure of the asymmetry of the distribution, whereas the kurtosis measures the dominance of the tails of the distribution. For a Gaussian distribution, the skewness is zero and the kurtosis is three. In the present study, we study the nonlinear effects by two-dimensional bathymetry that trigger non-Gaussian statistics indicated by the skewness and the kurtosis.

We use a Monte Carlo approach to estimate the statistical moments. We have performed numerical simulations multiple times with different incoming wave fields, i.e. wave fields generated from the same spectrum but with different random phases. From each simulation, we collect time series of surface elevation and horizontal velocity of length $100T_p$ in the domain of interest. The statistical moments are calculated by using time averaging first on the time series of length $100T_p$ then ensemble averaging from all different realisations.

A convergence study of the ensemble-averaged statistical moments with respect to the number of random runs was performed. As an example, we run 90 different realisations of case 3 in irregular waves over a circular shoal in § 4.1. Figure 4 shows the convergence of skewness and kurtosis with respect to the number of runs at the centre of the circular shoal. From these 90 realisations, we choose $n = 10, 20, 30$ and 40 random realisations and calculate the ensemble-averaged kurtosis of surface elevation. This process is repeated 100 times and we show the mean value, μ, and the standard deviation, σ, of averaged kurtosis of surface elevation in figure 5. We decided that 40 realisations is sufficient to have reliable estimates of the skewness and kurtosis.

4. Results

4.1. *Irregular waves over a circular shoal*

Long-crested irregular waves propagating over a circular shoal in computational domain with length 35 m and width 18 m is simulated by HOSM with truncation orders $M = 2$ and $M_B = 7$. The length of the damping zones are $\lambda_d = 5$ m at the left and right boundaries.
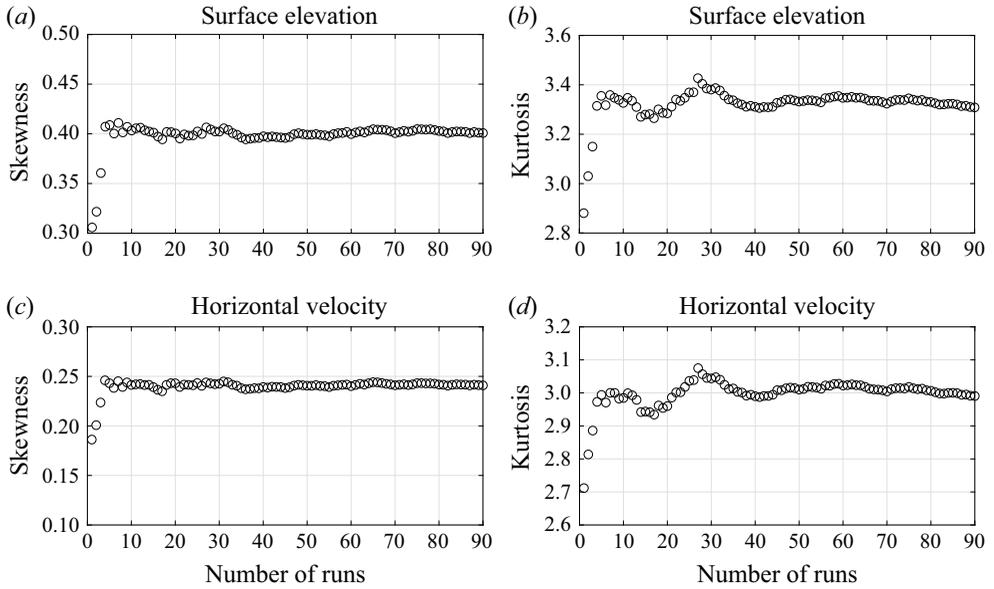
Figure 4. Convergence of the ensemble-averaged skewness and kurtosis of surface elevation and horizontal velocity at the centre of the circular shoal with respect to the number of runs.
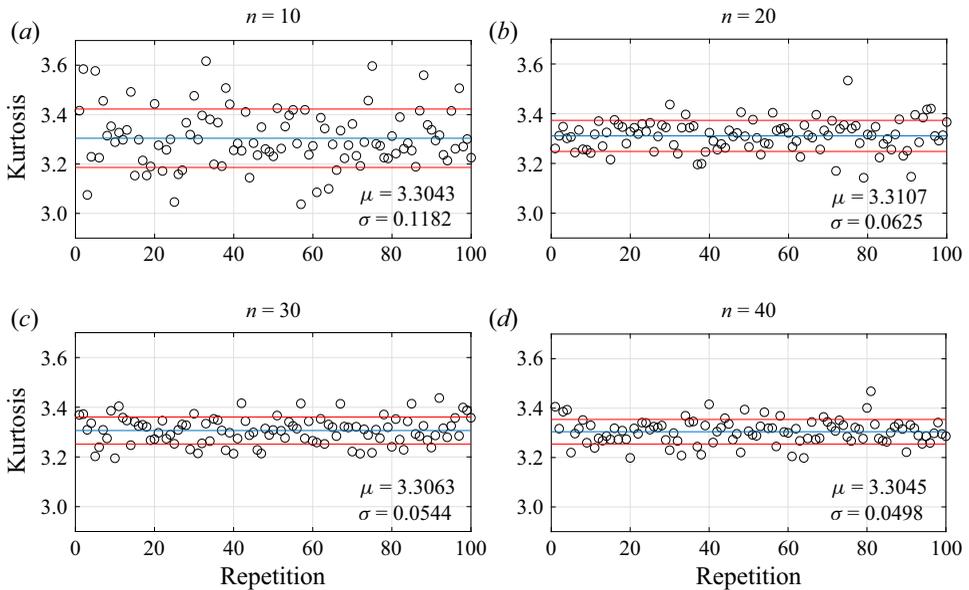

Figure 5. Averaged kurtosis of surface elevation from $n = 10, 20, 30$ and 40 random different runs. Here μ is the mean value and σ is the standard deviation from 100 repetitions.

The damping coefficient was set to $c_d = 1\,\mathrm{s}^{-1}$. The wave generator is located inside the domain at $x = 8\,\mathrm{m}$. The number of wave components in x and y directions are $N_x = 512$ and $N_y = 32$, respectively. The numerical simulation used similar bathymetry as the experiments of Chawla & Kirby (1996), but with a different radius. The horizontal velocity is calculated at $z = -0.04\,\mathrm{m}$. A sketch of the computational domain is given in figure 6.
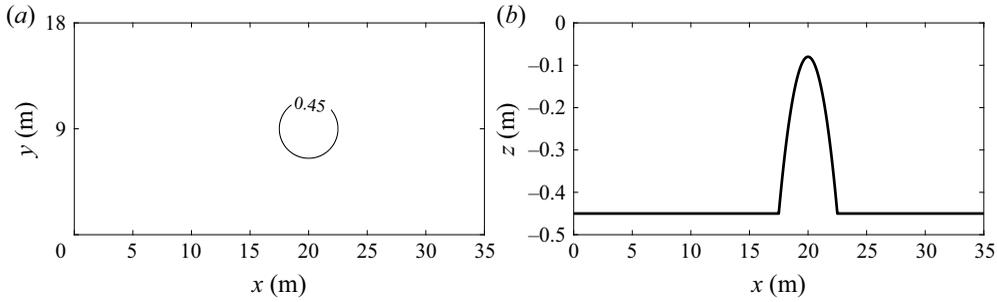
939 A41-8

Figure 6. Bottom topography of circular shoal with radius 2.5 m: (*a*) bottom contour; (*b*) centreline depth.

Case	R_{shoal} (m)	T_p (s)	H_s (cm)	$k_p a_c$	a_c/h	$k_p h_0$	$k_p h_{top}$
1	5	1	1	0.015	0.008	1.89	0.6
2	3.75	1	1	0.015	0.008	1.89	0.6
3	2.5	1	1	0.015	0.008	1.89	0.6
4	2.5	1	0.5	0.007	0.004	1.89	0.6
5	2.5	1	1.5	0.022	0.012	1.89	0.6

Table 1. Key parameters for irregular waves over a circular shoal simulation.

The circular shoal has a radius of R_{shoal} and the centre is located at $x = 20$ and $y = 9$ m. The water depth on the shoal is given by

$$h = h_0 + R_{sphere} - 0.37 - \sqrt{R_{sphere}^2 - (x - 20)^2 - (y - 9)^2}, \tag{4.1}$$

where $R_{sphere} = (R_{shoal}^2 + 0.37^2)/(2 \times 0.37)$, $h_0 = 0.45$ m is the constant water depth and the water depth on top of the shoal is $h_{top} = 0.08$ m. All numbers in (4.1) and R_{sphere} have unit of length meters (m).

The incoming wave field has a JONSWAP spectrum with peak period $T_p = 1$ s, significant wave height H_s and peak enhancement factor $\gamma = 3.3$. The non-dimensional depth $k_p h$ on the flat bottom part is 1.89 and on top of the shoal it is 0.6, where k_p is the corresponding peak wavenumber calculated from the peak period based on the linear dispersion relation. The steepness parameters are $k_p a_c = 0.0149$ and $a_c/h_0 = 0.0079$, where $a_c = \sqrt{2}\sigma$ is the characteristic amplitude and $\sigma = H_s/4$ is the standard deviation of the surface elevation. The characteristic wavelength $\lambda_p = 2\pi/k_p$ is 1.49 m. The parameters are summarised in table 1. The evolution of the power spectral density of the surface elevation and the horizontal velocity is included in the Appendix for Case 3.

Figures 7 and 8 show the statistics of the surface elevation and the horizontal velocity for irregular waves propagating over a circular shoal with different radii. The skewness has a local maximum on top of the shoal but not in the centre of the shoal, and has a local minimum on the lee side of the shoal. The skewness of the surface elevation and the horizontal velocity have the same trend. However, the surface elevation and the horizontal velocity have completely different behaviours for the kurtosis. The kurtosis of the surface elevation has a local maximum on top of the shoal, whereas the horizontal velocity has two local maxima of kurtosis at different locations on the lee side of the shoal. It is also noted that the kurtosis of surface elevation has other local maxima on the lee side of the shoal.
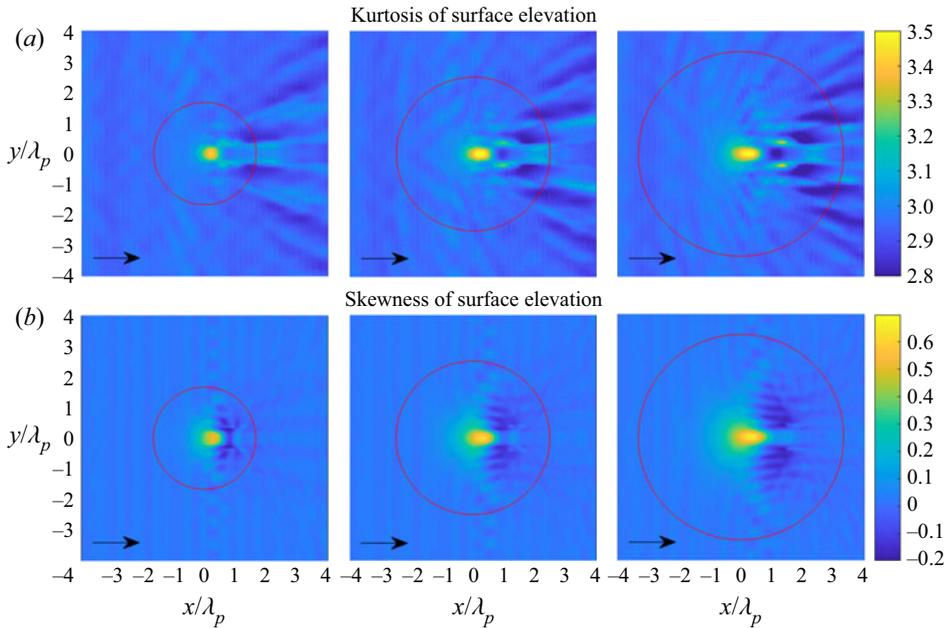
939 A41-9

Figure 7. (*a*) Kurtosis of surface elevation and (*b*) skewness of surface elevation for irregular waves over a circular shoal with $R_{shoal} = 2.5$, 3.75 and 5 m (from left to right). The red circle indicates the edge of the shoal at constant depth.
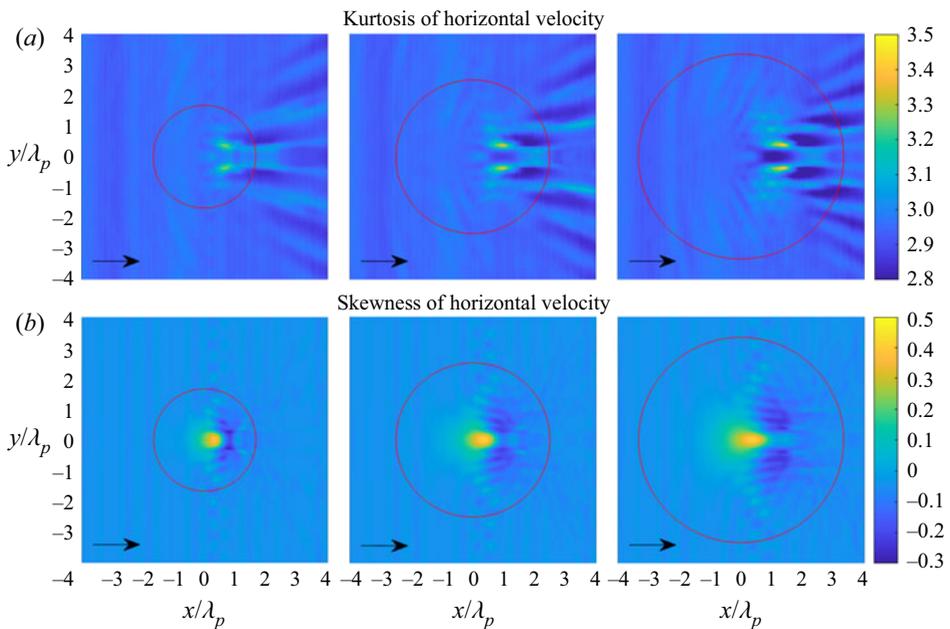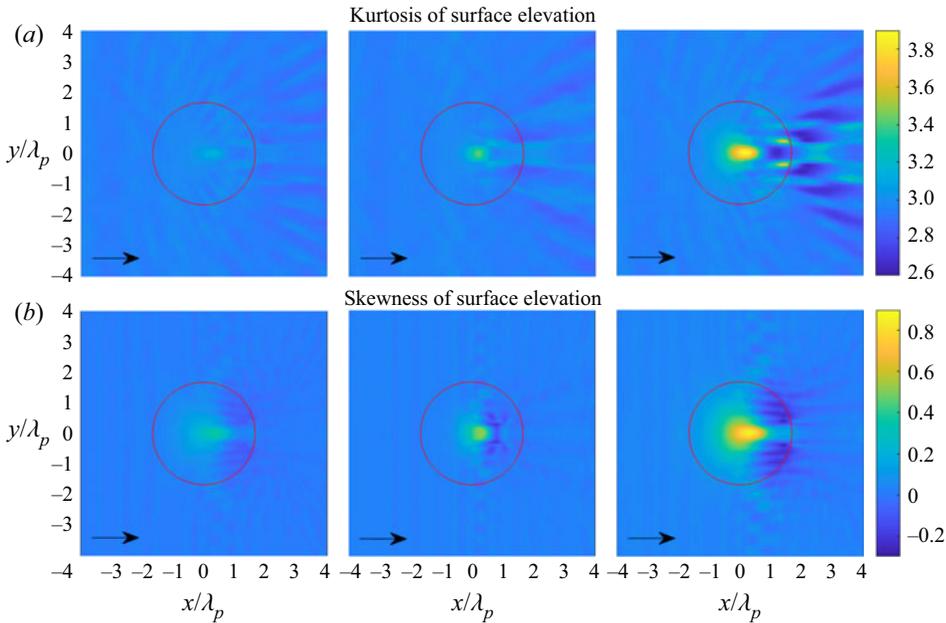

Figure 8. (*a*) Kurtosis of horizontal velocity and (*b*) skewness of horizontal velocity for irregular waves over a circular shoal with $R_{shoal} = 2.5$, 3.75 and 5 m (from left to right). The red circle indicates the edge of the shoal at constant depth.

Figure 9. (*a*) Kurtosis of surface elevation and (*b*) skewness of surface elevation for irregular waves over a circular shoal with $H_s = 0.5$, 1 and 1.5 cm (from left to right). The red circle indicates the edge of the shoal at constant depth.

Figures 9 and 10 show the statistics of the surface elevation and the horizontal velocity for irregular waves propagating over a circular shoal with same radius $R_{shoal} = 2.5$ m, but with different significant wave height H_s. The skewness of surface elevation and horizontal velocity still have the same trend with a local maximum on top of the shoal and a local minimum on the lee side of the shoal. For the highest significant wave height $H_s = 1.5$ cm, it is observed that the kurtosis of surface elevation has local maxima on top of the shoal and on the lee side of the shoal. Meanwhile, the kurtosis of horizontal velocity only has local maxima on the lee side of the shoal.

4.2. *Irregular waves over a semicircular step*

Long-crested irregular waves propagating over a submerged bar with a semicircular step in a periodic computational domain with length 40 m and width 18 m is simulated by the HOSM with same setup as in § 4.1.

We consider two types of bottom topography in this subsection. First, a submerged bar similar to the experiment by Trulsen *et al.* (2020), but with a semicircular step on the lee side, see figure 11. Second, a submerged bar with a semicircular step on the front and longer distance in the shallower part, see figure 12. The radius of the semicircle is 3 m. The water depth h_0 on the deeper part is 0.53 m and the water depth on the shallower part is 0.11 m. The horizontal velocity is calculated at $z = -0.055$ m.

For both cases, the incoming wave field has a JONSWAP spectrum with peak period $T_p = 1.1$ s, significant wave height $H_s = 2.5$ cm and peak enhancement factor $\gamma = 3.3$ similar to run 3 in Trulsen *et al.* (2020). The non-dimensional depth $k_p h$ on the deeper part is 1.85 and on the shallower part is 0.64. The steepness parameters are $k_p a_c = 0.0123$ and $a_c/h_0 = 0.0067$. The characteristic wavelength $\lambda_p = 2\pi/k_p$ is 1.8 m.
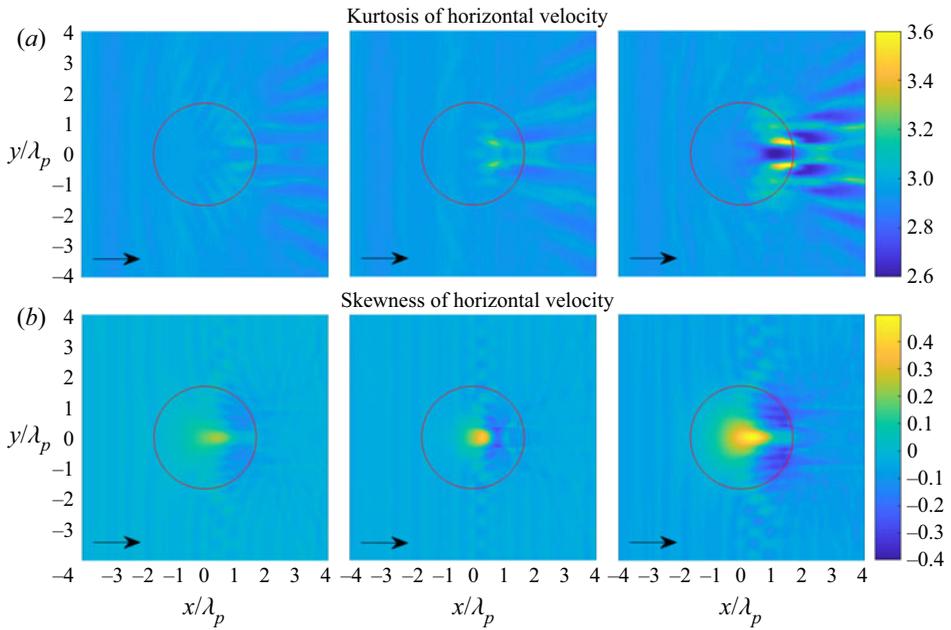
Figure 10. (*a*) Kurtosis of horizontal velocity and (*b*) skewness of horizontal velocity for irregular waves over a circular shoal with $H_s = 0.5$, 1 and 1.5 cm (from left to right). The red circle indicates the edge of the shoal at constant depth.
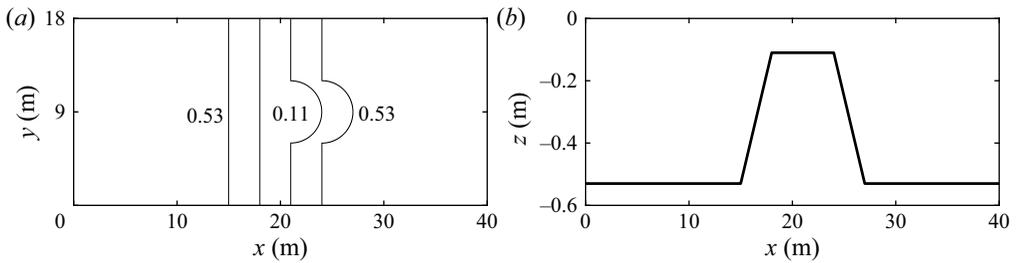

Figure 11. Bottom topography of submerged bar with semicircular step behind: (*a*) bottom contours; (*b*) centreline depth.
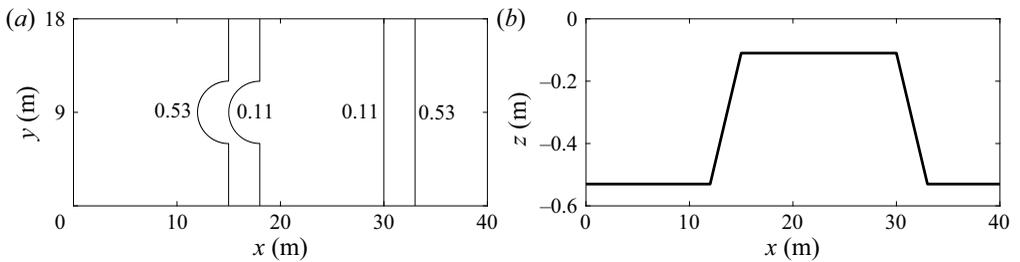

Figure 12. Bottom topography of submerged bar with semicircular step in front: (*a*) bottom contours; (*b*) centreline depth.
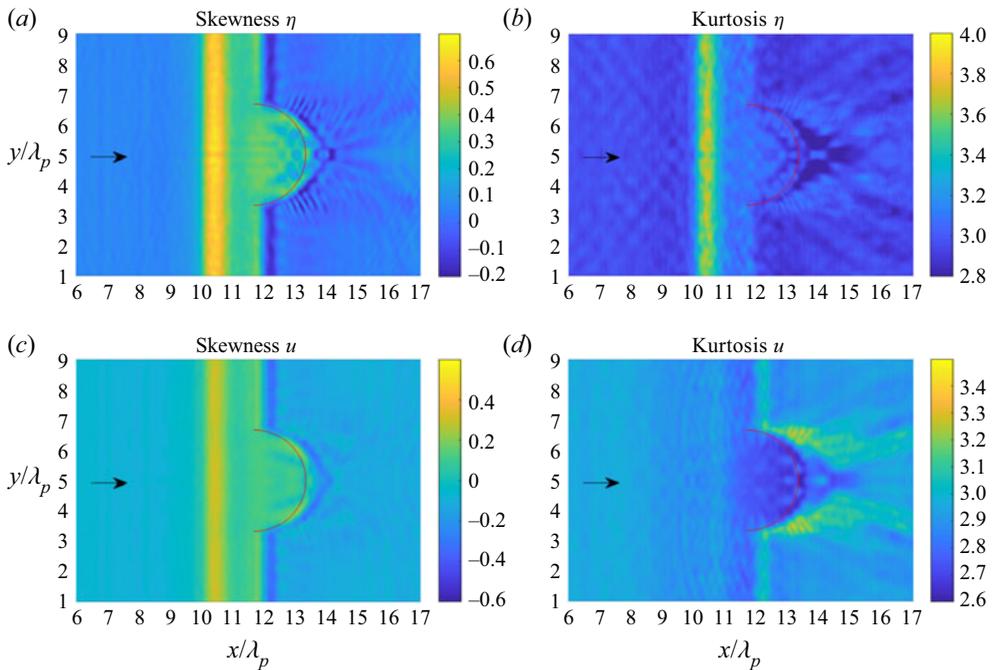
Figure 13. (*a*), (*c*) Skewness and (*b*), (*d*) kurtosis of (*a*), (*b*) surface elevation and (*c*), (*d*) horizontal velocity of irregular waves propagating over a submerged bar with a semicircular step behind. The red curve indicates the edge of the semicircular step on the shallower depth.

Figures 13 and 14 show the skewness and kurtosis of the surface elevation and the horizontal velocity for the submerged bar with a semicircular step on the lee side and on the front, respectively.

In figure 13, the skewness of the surface elevation and the horizontal velocity have the same behaviour. The skewness has local maximum on the shallower part of the bar and has a local minimum on the downslope. The kurtosis of surface elevation also has local maximum on the shallower part of the bar. Meanwhile, the kurtosis of horizontal velocity has different behaviour. There are increases in kurtosis of horizontal velocity on the downslope of semicircular step on the lee side.

In figure 14, the skewness of the surface elevation and the horizontal velocity has the same trend. The skewness has a local maximum after the edge of the upslope on the shallower part and also after some distance on the shallower part along the centreline. The kurtosis of the surface elevation has a local maximum after the edge of the upslope on the shallower part and also after some distance on the shallower part. On the other hand, the kurtosis of horizontal velocity has local maxima at different locations than the surface elevation. We notice there is a pattern for the kurtosis after some distance from the semicircular step on the front.

5. Discussion

Our numerical simulations confirm that non-uniform bathymetry can produce non-Gaussian statistics for both surface elevation and horizontal velocity. The statistical properties of the surface elevation and horizontal velocity can be different when the waves propagate over a varying bathymetry.
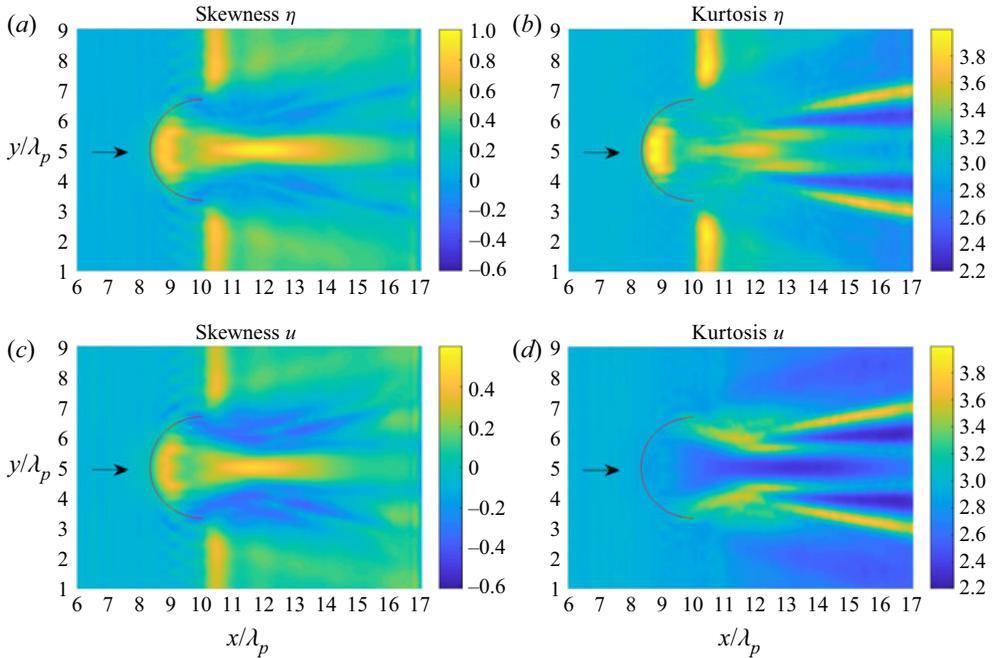
Figure 14. (*a*), (*c*) Skewness and (*b*), (*d*) kurtosis of (*a*), (*b*) surface elevation and (*c*), (*d*) horizontal velocity of irregular waves propagating over a submerged bar with a semicircular step in front. The red curve indicates the edge of the semicircular step on the shallower depth.

For irregular waves propagating over a circular shoal, the skewness of the surface elevation and horizontal velocity have local maxima on top of the shoal followed by a local minimum on the lee side of the shoal. The kurtosis of the surface elevation has a local maximum on top the shoal. This result is similar to the one-dimensional case reported experimentally in Trulsen *et al.* (2020) and numerically in Lawrence *et al.* (2021*b*). Unexpectedly, the kurtosis of surface elevation can have other local maxima on the lee side of the shoal and the kurtosis of the horizontal velocity also has two local maxima on the lee side of the shoal. It seems the two-dimensional effects from bottom topography such as refraction and diffraction influence the kurtosis of the surface elevation and the horizontal velocity.

For our cases with different bottom topography, a submerged bar with a semicircular step on the lee side acts similar to a focusing lens where the waves propagate from shallower to deeper water. The kurtosis of horizontal velocity has a significant increase not in the centre but on the left and right side from the direction of incoming waves of semicircular step as shown in figure 13. On the other hand, a submerged bar with a semicircular step on the front also acts similar to a focusing lens but from deeper to shallower water. After some distance from the edge of the semicircular step, in the area of the focal zone, there is a huge increase in the skewness of the surface elevation and the horizontal velocity. The kurtosis of the surface elevation has a local maximum around the centreline, whereas the kurtosis of the horizontal velocity has positive excess kurtosis not close to the centreline as shown in figure 14.

Our results suggest that the two-dimensional bathymetry affects the skewness and the kurtosis for both surface elevation and horizontal velocity.
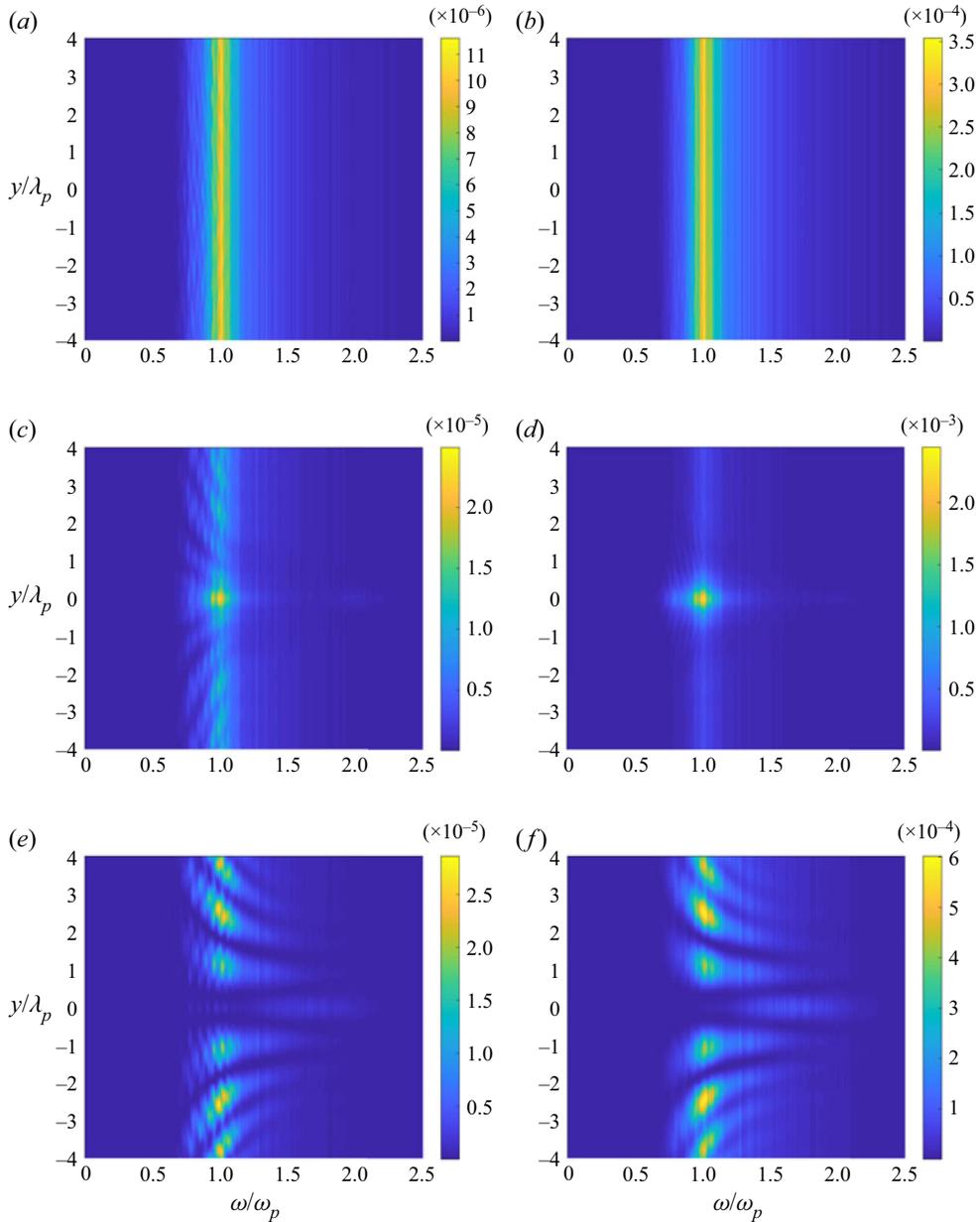
Figure 15. (*a*), (*c*), (*e*) Power spectral density of the surface elevation and (*b*), (*d*), (*f*) horizontal velocity of case 3 with irregular waves propagating over a shoal at $x = 15\,\text{m}$ (before the shoal, *a* and *b*), $x = 20\,\text{m}$ (centre of the shoal, *c* and *d*) and $x = 25\,\text{m}$ (after the shoal, *e* and *f*).

6. Summary and conclusion

We have performed a numerical study of the statistical properties of the surface elevation and the velocity field of long-crested irregular waves propagating over a two-dimensional bathymetry with a Monte Carlo approach. The statistical properties were studied in terms of evolution of the skewness and the kurtosis. The numerical simulations were performed using the HOSM for varying bottom from Gouin *et al.* (2017). We considered two types of bathymetry: a circular shoal and submerged bar with a semicircular step.

For our circular shoal, the depth transition is from $k_p h = 1.89$ to $k_p h = 0.6$. It has been found that the skewness of surface elevation and horizontal velocity have the same trend: a local maximum on top of the shoal and a local minimum on the lee side of the shoal. However, the kurtosis of surface elevation can have a local maximum on top of the shoal and local maxima on the lee side of the shoal. Meanwhile, the kurtosis of horizontal velocity only has two local maxima on the lee side of the shoal.

For our submerged bar with a semicircular step, the depth transition is from $k_p h = 1.85$ to $k_p h = 0.64$. Without the semicircular step, the submerged bar itself is similar to the experiment by Trulsen *et al.* (2020). We first considered submerged bar with a semicircular step on the lee side. In the area of the semicircular step on the lee side, the kurtosis of horizontal velocity increases at two locations similar to the previous case of a circular shoal. Second, we considered a submerged bar with a semicircular step on the front and longer distance in the shallower part. We have found that the skewness of the surface elevation and horizontal velocity have a significant increase after the edge of the upslope and also after some distance on the shallower part along the centreline. The kurtosis of the surface elevation has local maxima just after the edge of the upslope and after some distance on the shallower part. Meanwhile, the kurtosis of the horizontal velocity has local maxima not close to the centreline.

We conclude that two-dimensional bathymetry can trigger a significant increase in both skewness and kurtosis of surface elevation and horizontal velocity. The skewness of surface elevation and horizontal velocity have similar behaviour but the kurtosis of surface elevation and horizontal velocity can have completely different behaviours.

Declaration of interests. The authors report no conflict of interest.

Author ORCIDs.

ⓘ Christopher Lawrence https://orcid.org/0000-0002-5799-7089;

ⓘ Karsten Trulsen https://orcid.org/0000-0002-3070-3829;

ⓘ Odin Gramstad https://orcid.org/0000-0001-7531-3595.

Appendix

Figure 15 shows the power spectral density of the surface elevation and the horizontal velocity for case 3 with irregular waves propagating over a circular shoal. The power spectral density is calculated from an ensemble average of 40 different realisations.

REFERENCES

ALBERELLO, A., CHABCHOUB, A., GRAMSTAD, O., BABANIN, A.V. & TOFFOLI, A. 2016 Non-Gaussian properties of second-order wave orbital velocity. *Coast. Engng* **110**, 42–49.

BATEMAN, W.J.D., SWAN, C. & TAYLOR, P.H. 2003 On the calculation of the water particle kinematics arising in a directionally spread wavefield. *J. Comput. Phys.* **186** (1), 70–92.

BEJI, S. & BATTJES, J.A. 1993 Experimental investigation of wave propagation over a bar. *Coast. Engng* **19** (1), 151–162.

BERKHOFF, J.C.W., BOOIJ, N. & RADDER, A.C. 1982 Verification of numerical wave propagation models for simple harmonic linear water waves. *Coast. Engng* **20**, 255–279.

BITNER, E.M. 1980 Non-linear effects of the statistical model of shallow-water wind waves. *Appl. Ocean Res.* **2**, 63–73.

BOLLES, C.T., SPEER, K. & MOORE, M.N.J. 2019 Anomalous wave statisics induced by abrupt depth change. *Phys. Rev. Fluids* **4**, 011801.

CHAWLA, A. & KIRBY, J.T. 1996 Wave transformation over a submerged shoal. *CACR Rep. No.* 96-03, Department of Civil Engineering, University of Delaware.

CHERNEVA, Z., PETROVA, P., ANDREEVA, N. & GUEDES SOARES, C. 2005 Probability distributions of peaks, troughs and heights of wind waves measured in the black sea coastal zone. *Coast. Engng* **52**, 599–615.

DOMMERMUTH, D.G. & YUE, D.K.P. 1987 A high-order spectral method for the study of nonlinear gravity waves. *J. Fluid Mech.* **184**, 267–288.

DUCROZET, G. & GOUIN, M. 2017 Influence of varying bathymetry in rogue wave occurrence within unidirectional and directional sea-states. *J. Ocean Engng Mar. Energy* **3**, 309–324.

DUTYKH, D. & CLAMOND, D. 2014 Efficient computation of steady solitary gravity waves. *Wave Motion* **51**, 86–99.

DYSTHE, K., KROGSTAD, H.E. & MÜLLER, P. 2008 Oceanic rogue waves. *Annu. Rev. Fluid Mech.* **40** (1), 287–310.

FENTON, J.D. 1985 A 5th-order stokes theory for steady waves. *ASCE J. Waterway Port Coastal Ocean Engng* **111** (2), 216–234.

GOUIN, M., DUCROZET, G. & FERRANT, P. 2016 Development and validation of a non-linear spectral model for water waves over variable depth. *Eur. J. Mech.* B/*Fluids* **57**, 115–128.

GOUIN, M., DUCROZET, G. & FERRANT, P. 2017 Propagation of 3D nonlinear waves over an elliptical mound with a high-order spectral method. *Eur. J. Mech.* B/*Fluids* **63**, 9–24.

GRAMSTAD, O., ZENG, H., TRULSEN, K. & PEDERSEN, G.K. 2013 Freak waves in weakly nonlinear unidirectional wave trains over a sloping bottom in shallow water. *Phys. Fluids* **25**, 122103.

GRUE, J. 1992 Nonlinear water waves at a submerged obstacle or bottom topography. *J. Fluid Mech.* **244**, 455–476.

HAVER, S. 2000 Evidence of the existence of freak waves. In *Rogue Waves 2000* (ed. M. Olagnon & G. Athanassoulis), pp. 129–140. Ifremer.

JANSSEN, T.T. & HERBERS, T.H.C. 2009 Nonlinear wave statistics in a focal zone. *J. Phys. Oceanogr.* **39**, 1948–1964.

JANSSEN, T.T., HERBERS, T.H.C. & BATTJES, J.A. 2006 Generalized evolution equations for nonlinear surface gravity waves over two-dimensional topography. *J. Fluid Mech.* **552**, 393–418.

JANSSEN, T.T., HERBERS, T.H.C. & BATTJES, J.A. 2008 Evolution of ocean wave statistics in shallow water: refraction and diffraction over seafloor topography. *J. Geophys. Res.* **113**, C03024.

KASHIMA, H., HIRAYAMA, K. & MORI, N. 2014 Estimation of freak wave occurrence from deep to shallow water regions. *Coast. Engng. Proc.* **1** (34), waves.36.

KLAHN, M., MADSEN, P.A. & FUHRMAN, D.R. 2021a On the statistical properties of inertia and drag forces in nonlinear multi-directional irregular water waves. *J. Fluid Mech.* **916**, A59.

KLAHN, M., MADSEN, P.A. & FUHRMAN, D.R. 2021b On the statistical properties of surface elevation, velocities and accelerations in multi-directional irregular water waves. *J. Fluid Mech.* **910**, A23.

LAWRENCE, C., GRAMSTAD, O. & TRULSEN, K. 2021a Variational Boussinesq model for kinematics calculation of surface gravity waves over bathymetry. *Wave Motion* **100**, 102665.

LAWRENCE, C., TRULSEN, K. & GRAMSTAD, O. 2021b Statistical properties of wave kinematics in long-crested irregular waves propagating over non-uniform bathymetry. *Phys. Fluids* **3**, 046601.

LI, Y., DRAYCOTT, S., ADCOCK, T.A.A. & VAN DEN BREMER, T.S. 2021a Surface wavepackets subject to an abrupt depth change. Part 2. Experimental analysis. *J. Fluid Mech.* **915**, A72.

LI, Y., DRAYCOTT, S., ZHENG, Y.K., LIN, Z.L., ADCOCK, T.A.A. & VAN DEN BREMER, T.S. 2021b Why rogue waves occur atop abrupt depth transitions. *J. Fluid Mech.* **919**, R5.

LI, Y., ZHENG, Y.K., LIN, Z.L., ADCOCK, T.A.A. & VAN DEN BREMER, T.S. 2021c Surface wavepackets subject to an abrupt depth change. Part 1. Second-order theory. *J. Fluid Mech.* **915**, A71.

LIE, S.L., ADYTIA, D. & VAN GROESEN, E. 2014 Embedded wave generation for dispersive surface wave models. *Ocean Engng* **80**, 73–83.

MA, Y., DONG, G. & MA, X. 2014 Experimental study of statistics of random waves propagating over a bar. *Coast. Engng Proc.* **1** (34), waves.30.

MAJDA, A.J., MOORE, M.N.J. & QI, D. 2019 Statistical dynamical model to predict extreme events and anomalous features in shallow water waves with abrupt depth change. *Proc. Natl Acad. Sci. USA* **116**, 3982–3987.

MOORE, N.J., BOLLES, C.T., MAJDA, A.J. & QI, D. 2020 Anomalous waves triggered by abrupt depth changes: laboratory experiments and truncated KdV statistical mechanics. *J. Nonlinear Sci.* **30**, 3235–3263.

SERGEEVA, A., PELINOVSKY, E. & TALIPOVA, T. 2011 Nonlinear random wave field in shallow water: variable Korteweg–de Vries framework. *Nat. Hazards Earth Syst. Sci.* **11** (2), 323–330.

SERGEEVA, A. & SLUNYAEV, A. 2013 Rogue waves, rogue events and extreme wave kinematics in spatio-temporal fields of simulated sea states. *Nat. Hazards Earth Syst. Sci.* **13**, 1579–1771.

SONG, J.B. & WU, Y.H. 2000 Statistical distribution of water-particle velocity below the surface layer for finite water depth. *Coast. Engng* **40** (1), 1–19.

TEUTSCH, I., WEISSE, R., MOELLER, J. & KRUEGER, O. 2020 A statistical analysis of rogue waves in the southern North Sea. *Nat. Hazards Earth Syst. Sci.* **20** (10), 2665–2680.

TRULSEN, K., RAUSTØL, A., JORDE, S. & RYE, L.B. 2020 Extreme wave statistics of long-crested irregular waves over a shoal. *J. Fluid Mech.* **882**, R2.

TRULSEN, K., ZENG, H. & GRAMSTAD, O. 2012 Laboratory evidence of freak waves provoked by non-uniform bathymetry. *Phys. Fluids* **24** (9), 097101.

VIOTTI, C. & DIAS, F. 2014 Extreme waves induced by strong depth transitions: fully nonlinear results. *Phys. Fluids* **26**, 051705.

WANG, A., LUDU, A., ZONG, Z., ZOU, L. & PEI, Y. 2020 Experimental study of breathers and rogue waves generated by random waves over non-uniform bathymetry. *Phys. Fluids* **32** (8), 087109.

WEST, B.J., BRUECKNER, K.A., JANDA, R.S., MILDER, D.M. & MILTON, R.L. 1987 A new numerical method for surface hydrodynamics. *J. Geophys. Res.* **92** (C11), 11803–11824.

WHALIN, R.W. 1971 The limit of application of linear wave refraction theory in a convergence zone. *Res. Rep. No.* H-71-3, U.S. Army Engineer Waterways Experimiment Station.

ZAKHAROV, V.E. 1968 Stability of periodic waves of finite amplitude on the surface of a deep fluid. *J. Appl. Mech. Tech. Phys.* **9**, 190–194.

ZENG, H. & TRULSEN, K. 2012 Evolution of skewness and kurtosis of weakly nonlinear unidirectional waves over a sloping bottom. *Nat. Hazards Earth Syst. Sci.* **12**, 631–638.

ZHANG, J. & BENOIT, M. 2021 Wave-bottom interaction and extreme wave statistics due to shoaling and de-shoaling of irregular long-crested wave trains over steep seabed changes. *J. Fluid Mech.* **912**, A28.

ZHANG, J., BENOIT, M., KIMMOUN, O., CHABCHOUB, A. & HSU, H.-C. 2019 Statistics of extreme waves in coastal waters: large scale experiments and advanced numerical simulations. *Fluids* **4** (99), 1–24.

ZHENG, Y.K., LIN, Z.L., LI, Y., ADCOCK, T.A.A., LI, Y. & VAN DEN BREMER, T.S. 2020 Fully nonlinear simulations of unidirectional extreme waves provoked by strong depth transitions: the effect of slope. *Phys. Rev. Fluids* **5**, 064804.